Control-Surface Deflection Effects on Aerodynamic Response Nonlinearities

Gregory A. Addington* and James H. Myatt†
Air Vehicles Directorate, Air Force Research Laboratory
Wright-Patterson AFB, OH

1.0 Abstract

A static wind tunnel test of the Innovative Controls Effectors (ICE 101) conceptual aircraft configuration was conducted in the Air Force Research Laboratory's Vertical Wind Tunnel. This entry characterized the increments to the aerodynamic loading provided by the various control surfaces while using a more finely-resolved test matrix in angle of attack and sideslip than typically seen in wind tunnel testing. The purpose for obtaining these data was to determine the effect which control surface deflection had on critical state locations in preparation for the test of a second ICE model built with remotely-actuated control surfaces. (Critical states are discrete flight mechanical states where the aerodynamic response looses its analytic dependence on one or more state variables.) These data demonstrate that the aerodynamic increments are in many cases at minimum nonlinear functions of the surface deflection angle, and strongly suggest that some critical states do shift in angle of attack and/or sideslip with changing deflection angle.

2.0 Nomenclature

AMT ..... All-Moving Tip
b ..... Trailing-Edge Wing Span (ft)
c ..... Mean Aerodynamic Chord (ft)
C_l ..... Rolling-Moment Coefficient, l/qSb
C_m ..... Pitching-Moment Coefficient, m/qSc
C_N ..... Normal-Force Coefficient, N/qS
C_n ..... Yawing-Moment Coefficient, n/qSb
ICE ..... Innovative Control Effectors
l ..... Rolling Moment (ft-lb)
LEF ..... Leading-Edge Flap
m ..... Pitching Moment (ft-lb)
MAT ..... Multi-Axis Test
N ..... Normal Force (lb)
n ..... Yawing moment (ft-lb)
PF ..... Pitch Flap
q ..... Freestream Dynamic Pressure (lb/ft^2)
S ..... Wing Area (ft^2)
SPLR ..... Spoiler
SSD ..... Spoiler Slot Deflector
TEF ..... Trailing-Edge Flap
VWT ..... AFRL Vertical Wind Tunnel
α ..... Wind-Axis Angle of Attack (deg)
β ..... Wind-Axis Sideslip Angle (deg)

3.0 Introduction

The Innovative Control Effectors (ICE) program,[1,2] conducted cooperatively between Wright Laboratory (now a part of Air Force Research Laboratory) and Lockheed Martin Tactical Aircraft Systems, developed a conceptual fighter configuration to fill the future USAF strike fighter mission. This aircraft was designed to be an agile multi-role fighter with significant low-observability features, necessitating a tailless design capable of flying at high angles of attack. The design developed by Lockheed-Martin Tactical Aircraft Systems, designated ICE 101, is an all-flying delta-wing configuration with a 65° leading-edge sweep and sawtooth trailing edge, as shown in Fig. 1. This design possesses five sets of control surfaces (see Fig. 2 and References 1 and 2): conventional leading-edge flaps; pitch flaps; trailing-edge flaps (elevons); all-moving tips; and spoiler slot deflectors (the upper surface of which can be used as a spoiler alone).

Research using a more generic 65° delta wing model has demonstrated that not only is the aerodynamic response a nonlinear function of the flight mechanical state variables, but it can change discontinuously with those variables.[3,4,5,6] These discontinuities, known as critical states, have been shown empirically to be related to bifurcations in the surrounding flow field, *e.g.*, coinciding with the onset of flow separation, leading-edge vortex burst, or the appearance / disappearance of more subtle flow structures.[6] Furthermore, the crossing of a critical state during one degree of freedom motions has been shown to introduce a transient in the aerodynamic response of remarkably long duration in addition to the slower-than-convective-time-scale response which results in the presence of vortex burst or stall onset.[4,5]

Given the similarity of the planforms between the ICE 101 and the basic 65° delta wing, the likelihood that the ICE 101 model would exhibit many of the same sorts of nonlinear and even discontinuous aerodynamic response characteristics is substantial and has indeed been shown to a small extent.[7] The dependence of critical state locations on the control surface deflections is unknown; however, as these surfaces affect the pressure gradient over the model surface, an effect on critical state locations was

---

* Aerospace Engineer; Senior Member AIAA
† Aerospace Engineer; Member AIAA

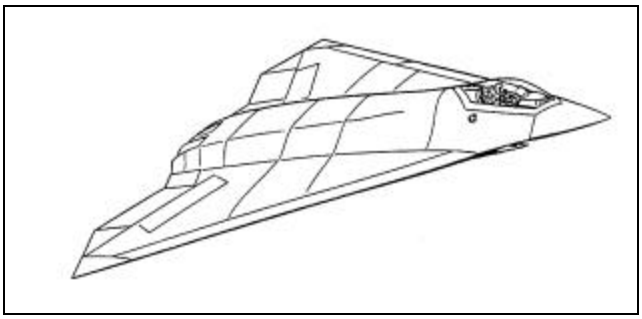

Fig. 1 ICE 101 Conceptual Aircraft Design.

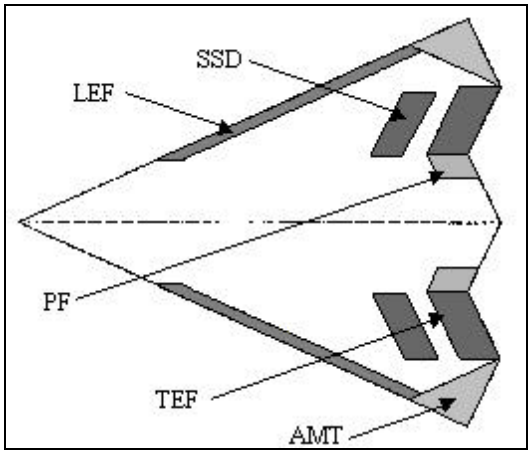

Fig. 2 ICE Control Effectors Approximate Locations (Not to Scale).

presumed likely. Should the control surfaces affect critical state locations or their transient response characteristics, the impact on the flight control law design could be significant. Given the potential impact that these effects would have on an air vehicle's design process, a wind tunnel test investigating these effects was warranted.

The data included in this report are the results from an entry into the AFRL Vertical Wind Tunnel using the lightweight ICE 101 rotary balance model. To isolate regions in the angle of attack – sideslip domain where the aerodynamic responses changed discontinuously with both those variables and control surface deflections, a test matrix was developed to have more finely-resolved increments in these variables than typically found in wind tunnel tests. These data were then reviewed for changes in discontinuity locations in the angle of attack – sideslip plane and for conditions where the aerodynamic responses appeared to be nonlinear functions of the control surface deflection angle. The conduct of this test was as described in the following section, which is followed by a limited discussion and summary of the results. The complete data set is found in the Appendices.

Although these data are useful in and of themselves, their primary use will be in guiding test matrix formulation for the testing of a geometrically-identical model with remotely-actuated control surfaces. In this test, the transient aerodynamic responses to control surface deflections will be measured in an effort to determine the correlation to control surface deflections, including nonlinearities in both time and surface deflection angle.

4.0 Experimental Procedures

This wind tunnel test was conducted in the AFRL Vertical Wind Tunnel located at Wright-Patterson AFB, OH. This facility is a closed-loop, open test section facility with a relatively low freestream turbulence level.

This test used the static capabilities of the VWT's Multi-Axis Test Rig. This rig is a framework which minimizes interference effects while allowing displacements in angle of attack and sideslip as well as wind-axis rotary and body-axis harmonic motion. A photograph of the MAT rig with the ICE lightweight model is shown in Fig. 3.

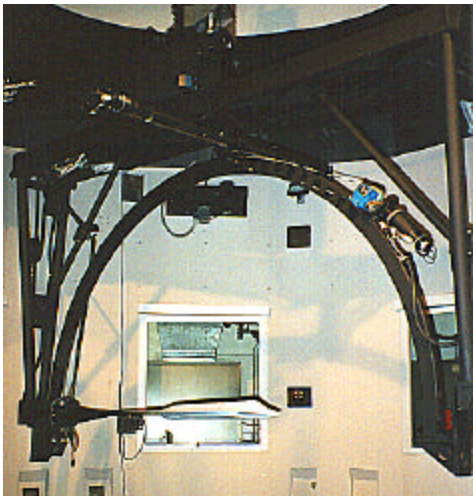

Fig. 3 The ICE 101 Lightweight Model in the VWT.

The lightweight ICE 101 rotary balance model was used as the test body. The model is constructed of fiberglass laid over a foam core and reinforced by balsa wood and plywood, making it sufficiently light as to avoid imparting significant inertial loads during dynamic testing at rates scaled with respect to model dimensions and freestream velocity yet strong enough not to yield at dynamic pressures of 5 psf and stiff enough not to deform during dynamic testing. This model also has movable control surfaces held in place by rods and set screws, which (with the exception of the SSD's which were fixed at neutral or maximum deflection only) may be set at any angle between their maximum deflection angles. Deflection angles were set using templates fit to each control surface.

These experiments were conducted at a wide range of

angle of attack and sideslip combinations, as detailed in Table 1. All data were acquired using a freestream dynamic pressure of 3 psf, which translates to an approximate freestream velocity of 50 fps (dependent on test section conditions) and a Reynolds number of 830,000 based on root chord. As is noted in Table 1, a portion of these data were acquired at sideslip angles of –20° to 0°, but to simplify their presentation they will be presented with the remaining data using positive sideslip angles. To convert these data, the sideslip angle, rolling moment coefficient and yawing moment coefficients were multiplied by –1, in following with anti-symmetry. For clarity and brevity, not all data are included in this report.

Table 1 Control surface deflection angles

Control Surface	**Deflection Angles** (left / right)	**b*** min:incr:max
Baseline (all surfaces neutral)	N/A	-20°:2°:20°
Leading-Edge Flap	10/0	-6°:2°:20°
	20/0	-6°:2°:20°
	30/0	-6°:2°:20°
	0/10	-6°:2°:20°
	0/30	-6°:2°:20°
	30/30	-6°:2°:20°
Pitch Flap	30/30	-6°:2°:20°
	-30/-30	-6°:2°:20°
Elevon	30/0	-6°:2°:20°
	-30/0	-6°:2°:20°
	0/30	-6°:2°:20°
	0/-30	-6°:2°:20°
	-30/30	-20°:2°:20°
All-Moving Tips	-10/0	-20°:2°:20°
	30/0	-20°:2°:20°
	60/0	-20°:2°:20°
	60/30	-20°:2°:20°
Spoiler	60/0	-20°:2°:20°
	60/60	-6°:2°:20°
Spoiler / Slot Deflector	60/0	-20°:2°:20°
	60/60	-6°:2°:20°

* - all data acquired for α = (0°:5°:45°)

5.0 Results

All of the cases presented in this section are examples of data which show a significant alteration of the nonlinear behavior and/or a change in the apparent critical state location as brought about by deflection of a control surface. However, in most of the conditions investigated the aerodynamic response was altered by a simple linear increment.

In the following discussion, the control surface deflection angles will be presented in the form *m*/*n*. In this format, *m* is the deflection of the left and *n* the right control surface. All deflections are given in degrees, with the free edge (AMT trailing edge) deflected downward being positive. Which of the control surfaces are being discussed will be listed immediately prior to the ratio or will be obvious from context as only one control surface or matching pair of surfaces was deflected at a time.

Throughout the discussion that follows, relatively sudden changes in the magnitude of the data or slope are referred to as (apparent) critical states. The resolution of angles of attack and sideslip at which these data where acquired prohibits discussing such conditions as critical states as, in most cases, a continuous function can be found which describes the data fully. However, such functions are well separated from the linear and quasi-linear functions which are typically used to describe such data. Nonetheless, although the following discussion uses the term “critical state” somewhat loosely, the reader is warned that such locations may not be true discontinuities but may merely be locations where the nonlinearity in the results changes its gross character.

5.1 Baseline Data

Fig. 4 – 8 display normal force, pitching moment, rolling moment and yawing moment data in coefficient form for the ICE 101 lightweight model with all control surfaces at their undeflected locations. In Fig. 4 normal-force coefficient data are shown as a function of angle of attack for β = 0° and 10°. Although these data are clearly nonlinear functions of angle of attack, they exhibit no obvious signs of containing discontinuities. However, the slope of these data change sign at $\alpha \approx 35°$, a characteristic which is associated with the loss of leading-edge suction on delta wing planforms. The disappearance of this structure would be a bifurcation in the flow field topology and hence would likely be a critical state.[6]

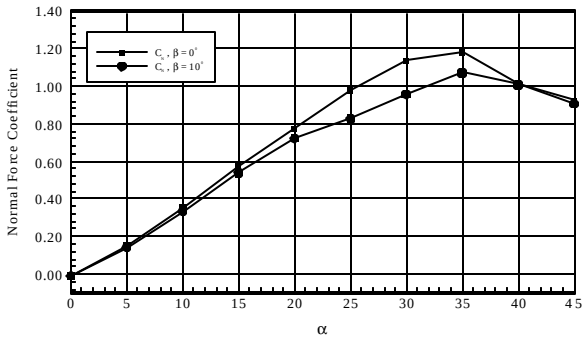

Fig. 4 Normal Force Coefficient as a Function of Angle of Attack, No Control Deflections, b = 0° and 10°

Figures 5 and 6 present pitching-moment, rolling-moment and yawing-moment coefficient as functions of angle of attack for β = 0° and 10°, respectively. These data contain more clear indications of the presence of critical states. In particular, the pitching-moment-coefficient data in Fig. 5 change slope at α = 10°, 30° and 40°; all three moments shown in Fig. 6 exhibited similar changes in slope at several different angles of attack. Obviously, a mere change in slope does not mean a critical state is present since continuous functions may easily fit these data. However, previous results strongly suggest that at least some of these locations are critical states, the sparseness of the data precluding a definitive statement.

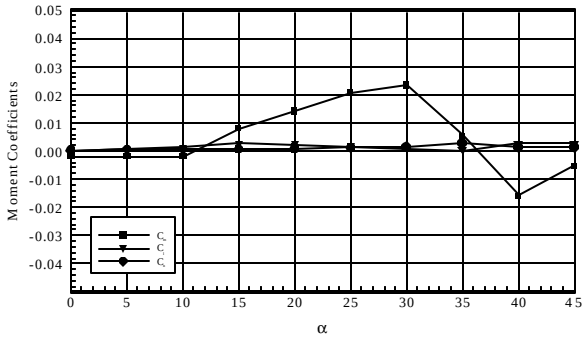

Fig. 5 Pitching-Moment, Rolling-Moment and Yawing-Moment Coefficients as a Function of Angle of Attack, No Control Deflections, b = 0°.

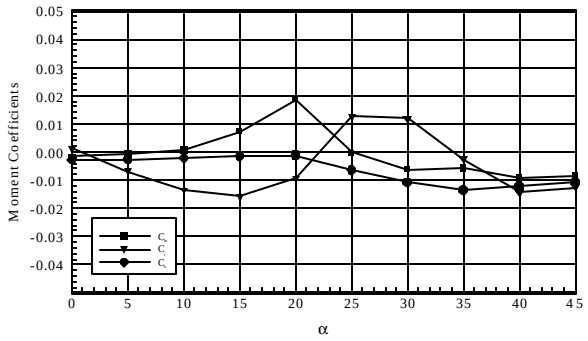

Fig. 6 Pitching-Moment, Rolling-Moment and Yawing-Moment Coefficients as a Function of Angle of Attack, No Control Deflections, b = 10°.

Finally, Figs. 7 and 8 present the same moment coefficients but as functions of sideslip angle for α = 20° and 25°. The data contained in these two figures demonstrate the magnitude of change a 5° increase in angle of attack can cause in the aerodynamic loading. The largest change occurs in pitching moment, with a large change in magnitude occurring between β = 8° and 10° for α = 25°. Such a large magnitude shift was observed in the 65° pure delta wing data, associated with the crossing of leading-edge vortex burst across the leeward trailing edge.[3,6] The character of the rolling moment coefficient also changed, indicating a large asymmetry in the flow field formed between α = 20° and 25°. Such an asymmetry would also be consistent with asymmetric vortex burst locations. This result was significant as leading-edge-vortex burst has been found to be a significant driving force of the aerodynamic loadings of delta wings and the nonlinearity of those loadings with respect to both the state variables of flight mechanics and time during dynamic testing.

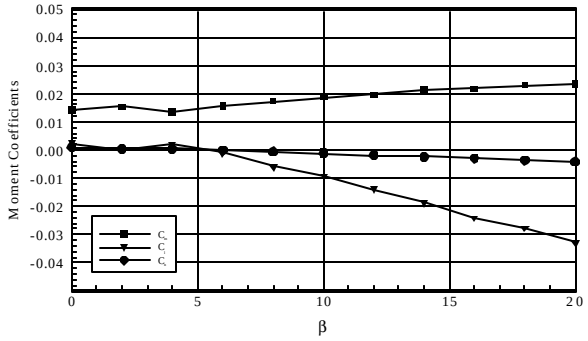

Fig. 7 Pitching-Moment, Rolling-Moment and Yawing-Moment Coefficients as a Function of Sideslip Angle, No Control Deflections, a = 20°.

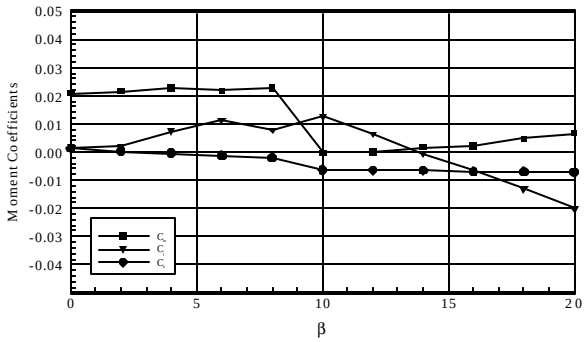

Fig. 8 Pitching-Moment, Rolling-Moment and Yawing-Moment Coefficients as a Function of Sideslip Angle, No Control Deflections, a = 25°.

5.2 LEF Deflections

Data acquired with the ICE LEF's configured at different combinations of deflection angles are shown in Figs. 9 – 13.

The data presented in Fig. 9 demonstrate that the pitching moment as a function of sideslip at $\alpha = 25°$ with different LEF configurations followed the same trend as for the baseline configuration case except for the 0/30 deflection. All data were of the same order of magnitude and general character for $\beta \leq 8°$. A large change in magnitude – an apparent critical state – exists between $8° < \beta < 10°$ for all LEF configurations except for the 0/30 deflection for which the change in magnitude is replaced by a protracted region of apparently-continuous positive slope. The remaining data showed little variation with LEF deflection with the exception of a small difference for the 0/10 deflection, indicating little control power throughout the sideslip range for the left LEF. The accompanying rolling-moment-coefficient data (Fig. 10) indicate that the apparent critical state which resides between $8° < \beta < 10°$ for most of the conditions tested was apparently shifted to between $4° < \beta < 6°$ for the 0/30 LEF setting. This shift would explain the transition to the nearly-constant negative slope at the smaller sideslip angle. Finally, yawing-moment-coefficient data (Fig. 11), like the pitching-moment-coefficient data, demonstrate that the effect of the apparent critical state between $8° < \beta < 10°$ was shifted or suppressed by the 0/30 LEF setting.

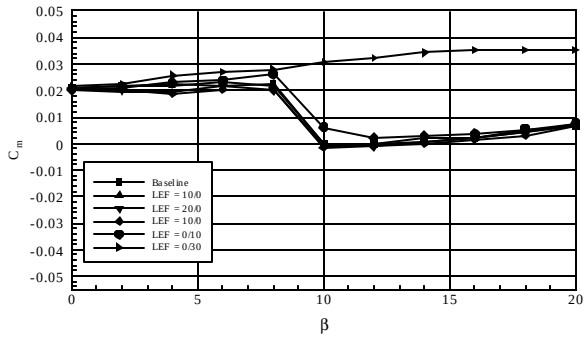

Fig. 9 Pitching-Moment Coefficient Data as a Function of Sideslip Angle with LEF Deflections, a = 25°.

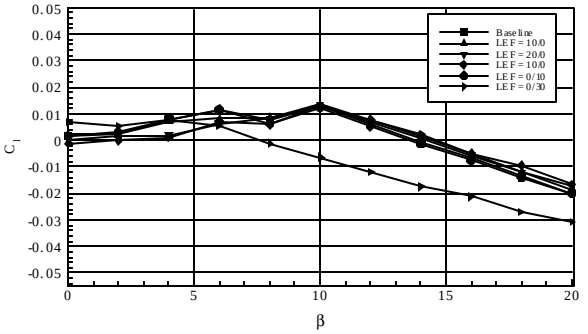

Fig. 10 Rolling-Moment Coefficient Data as a Function of Sideslip Angle with LEF Deflections, a = 25°.

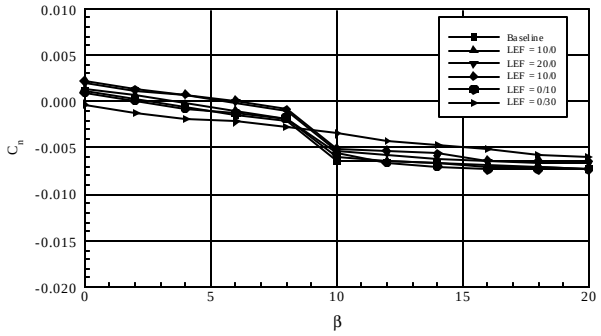

Fig. 11 Yawing-Moment Coefficient Data as a Function of Sideslip Angle with LEF Deflections, a = 25°.

Figures 12 and 13 present rolling-moment and yawing-moment-coefficient data as a function of angle of attack at zero sideslip. As was the case previously, all of the data followed the same trends except for those taken with the leading edge flap configuration 0/30. These data show that between $15° < \alpha < 30°$ the rolling moment coefficient deviated significantly from the remainder of the data, while yawing moment deviated in trend if not magnitude for all $\alpha > 5°$.

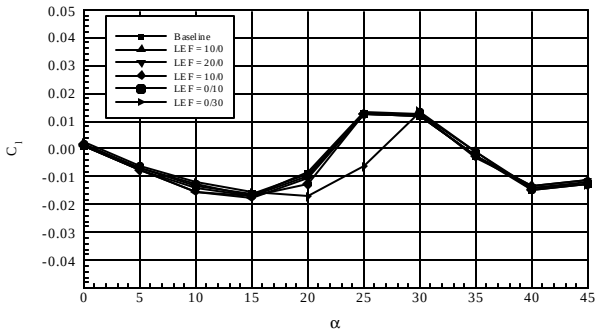

Fig. 12 Rolling-Moment Coefficient as a Function of Angle of Attack with LEF Deflections, b = 10°.

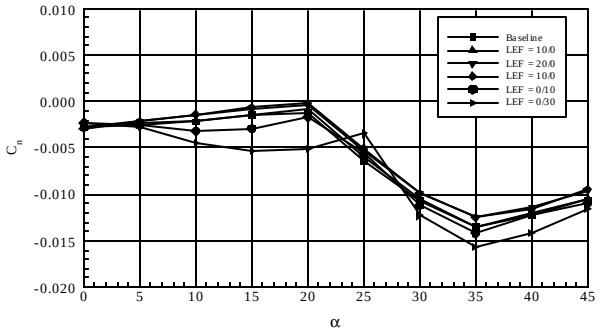

Fig. 13 Yawing-Moment Coefficient as a Function of Angle of Attack with LEF Deflections, b = 10°.

5.3 TEF Deflections

Data acquired with the ICE TEF's configured at different combinations of deflection angles are shown in Figs. 14 – 16.

The pitching-moment-coefficient data in Fig. 14 indicate that the critical state for the baseline configuration between 8° < β < 10°°for α = 25° was shifted by deflecting the trailing-edge flaps. TEF deflections of 0/-30 and –30/30 appear to shift this critical state to greater sideslip angles (between 10° and 12°), while a deflection of 30/0 appears to shift the large decrement to a lesser sideslip angle (between 6° and 8°). Furthermore, a deflection of 0/30 caused the decrement to slightly increase in total magnitude but lessen in apparent slope, with the total decrease in pitching moment occurring between β ≈ 8° and 12°. Whether this result indicates the suppression of the critical state, a splitting of the effect into a greater number of critical states or some other alteration of the phenomenon can not be determined without additional data.

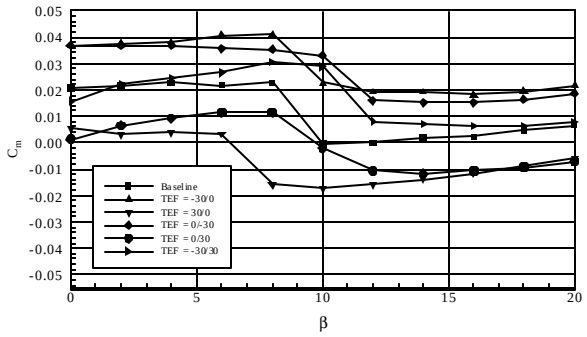

Fig. 14 Pitching-Moment Coefficient as a Function of Sideslip Angle with TEF Deflections, a = 25°.

Pitching- and rolling-moment-coefficient data acquired at β = 10° are shown as a function of sideslip in Figs. 15 and 16, respectively. In these data, the TEF deflections of 0/-30 and –30/30 appear to shift the respective maxima in pitching moment from α ≈ 20° to approaching 25°. The trends of the remaining data are comparable.

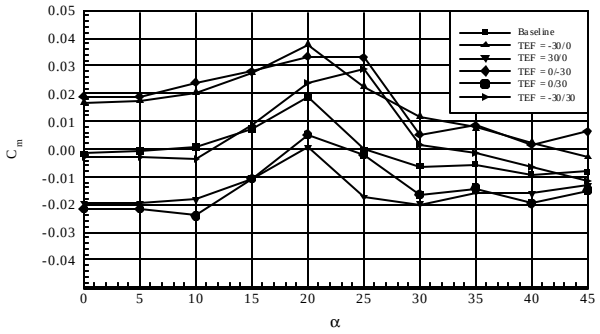

Fig. 15 Pitching-Moment Coefficient as a Function of Angle of Attack with TEF Deflections, b = 10°.

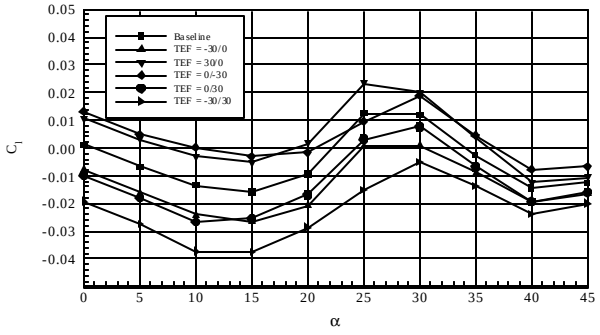

Fig. 16 Rolling-Moment Coefficient as a Function of Angle of Attack with TEF Deflections, b = 10°.

5.4 PF Deflections

Data acquired with the ICE PF's configured at different combinations of deflection angles are shown in Figs. 17 – 19.

Pitching-moment-coefficient data acquired at $\alpha = 25°$ are shown as a function of sideslip angle in Fig. 17. These data show that the large decrement in pitching-moment coefficient which occurs in the baseline data between $\beta = 8°$ and 10° is diffused over a larger range of sideslip angles for both pitch flap setting. Whether this apparent discontinuity is suppressed, mitigated or displaced for each deflection is not discernable without additional data.

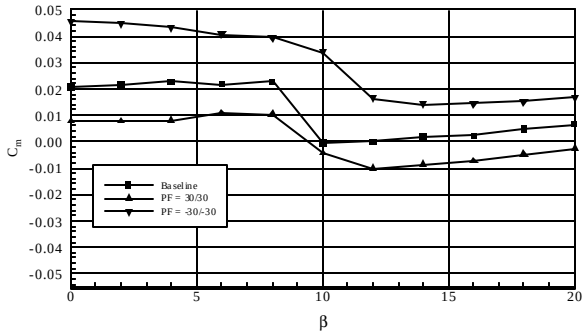

Fig. 17 Pitching-Moment Coefficient as a Function of Sideslip Angle with PF Deflections, $\alpha = 25°$.

Rolling-moment-coefficient data, both as a function of sideslip angle (Fig. 18) and angle of attack (Fig. 19) show that the -30/-30 pitch flap setting suppressed local peaks in these data. Similar to the pitching-moment-coefficient data, it is not clear whether one or more critical states have been averted, shifted, or some combination thereof.

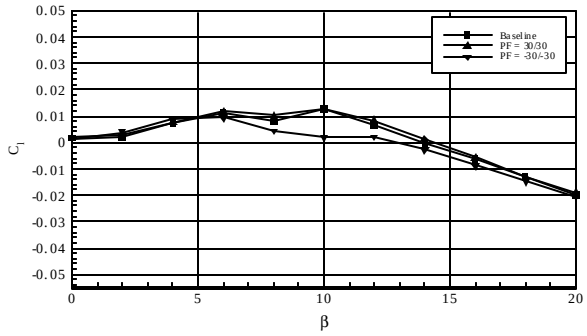

Fig. 18 Rolling-Moment Coefficient as a Function of Sideslip Angle with PF Deflections, $\alpha = 25°$.

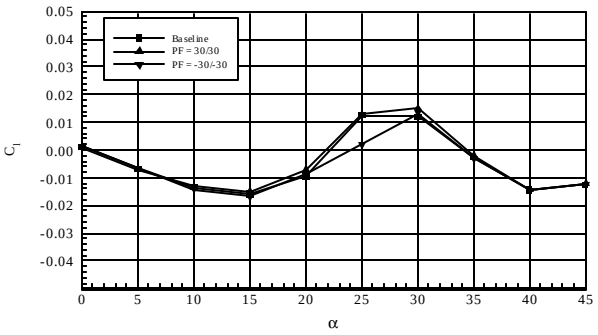

Fig. 19 Rolling-Moment Coefficient as a Function of Angle of Attack with PF Deflections, $\beta = 10°$.

5.5 AMT Deflections

Data acquired with the ICE AMT's configured at different combinations of deflection angles are shown in Figs. 20 and 21.

Figure 20 presents one of the few cases where an effect with significant nonlinear if not discontinuous behavior could be found at small sideslip angle and angle of attack. In these data for a constant 6° sideslip, the pitching-moment coefficient remains relatively flat in the baseline configuration and with the all-moving tips deflected to –10/0 for $\alpha \leq 10°$, but the data have a positive slope for deflections of 30/0, 60/0 and 60/60. All deflected-AMT data beyond $\alpha = 10°$ follow the baseline data trend, perhaps indicating a transition in the nature of the pitching moment's dependence on AMT deflection.

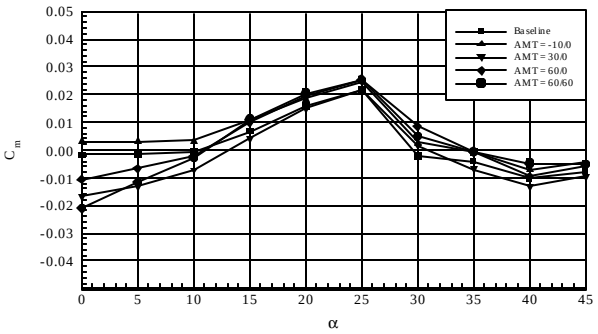

Fig. 20 Pitching-Moment Coefficient as a Function of Angle of Attack with AMT Deflections, $\beta = 6°$.

Figure 21 presents rolling-moment-coefficient data as a function of sideslip angle at a constant $\alpha = 25°$. These results show that AMT deflections of 60/0 and 60/60 cause a deviation in the trend of these data away from that of the baseline and other AMT deflections for $4° < \beta < 10°$. This alteration of the data trend may be indicative of a suppression of a critical state at $\beta \approx 2°$ or may be the result of a nonlinear dependence of rolling moment on AMT deflection.

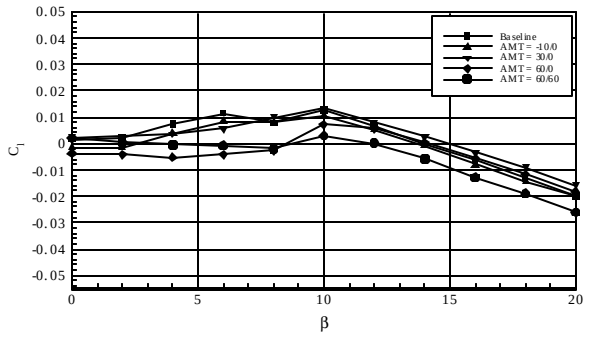

Fig. 21 Rolling-Moment Coefficient as a Function of Sideslip Angle with AMT Deflections, a = 25°.

5.6 Spoiler Deflections

Data acquired with the ICE spoilers configured at different combinations of deflection angles are shown in Figs. 22 – 24.

The pitching-moment-coefficient data shown in Figs. 22 and 23 indicate that the deployment of the spoiler(s) tended to delay the apparent critical states. In the pitching-moment-coefficient data, the discontinuity at $\beta \approx$ 8° - 10° and α = 25° (Fig. 22) and the peak at $\alpha \approx$ 20° for β = 10° (Fig. 23) were delayed by spoiler deployment, while the peak in rolling-moment coefficient between α = 25° and 30° for β = 10° was delayed to closer to 30° (Fig. 24).

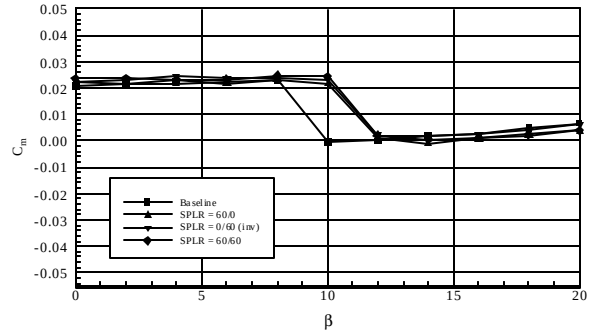

Fig. 22 Pitching-Moment Coefficient as a Function of Sideslip Angle with Spoiler-Alone Deflections, a = 25°

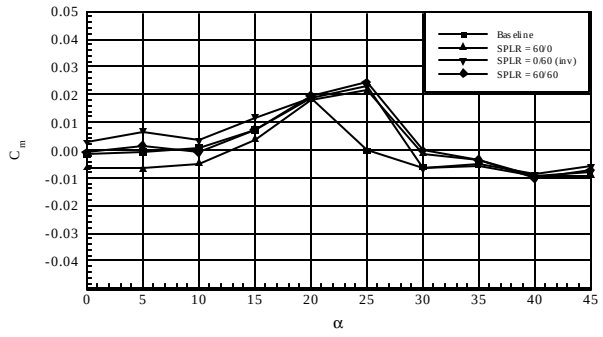

Fig. 23 Pitching-Moment Coefficient as a Function of Angle of Attack with Spoiler-Alone Deflections, b = 10°

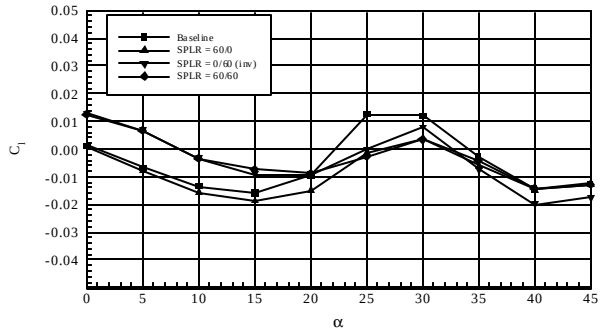

Fig. 24 Rolling-Moment Coefficient as a Function of Angle of Attack with Spoiler-Alone Deflections, b = 10°

5.7 SSD Deflections

Data acquired with the ICE SSD's configured at different combinations of deflection angles are shown in Figs. 25 and 26.

The pitching-moment-coefficient data shown in Fig. 25 indicate that the apparent critical state present in the baseline data at β = 8° – 10°, α = 25°, is delayed to greater sideslip angles and the magnitude of the decrement decreased with SSD deployment. Furthermore, the increment difference between the 60/0 and 60/60 configurations not only includes a magnitude change but also a shift in the apparent discontinuity (to between β = 14° – 16°), indicating some degree of interference between the two surfaces. Rolling-moment-coefficient-data shown in Fig. 26 indicate that the local maxima found in the baseline configuration data at β = 6° and 10° are suppressed.

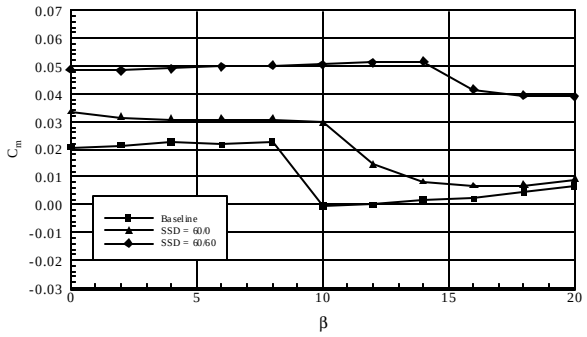

Fig. 25 Pitching-Moment Coefficient as a Function of Sideslip Angle with SSD Deflections, a = 25°

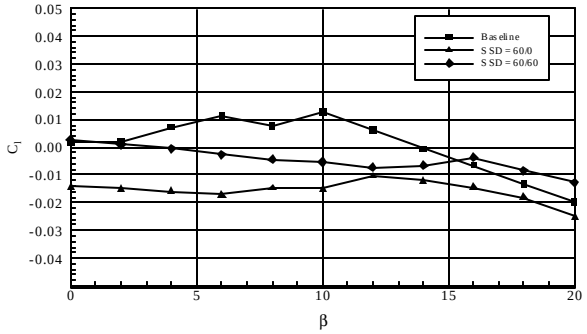

Fig. 26 Rolling-Moment Coefficient as a Function of Sideslip Angle with SSD Deflections, a = 25°

6.0 Discussion

Common practice in developing aerodynamic models for the aerodynamic increments provided by control surface deflections is to utilize a derivative coefficient, for example,

$$\Delta C_l = C_{l_{\delta_{AMT}}} * \delta_{AMT}$$

where

$$C_{l_{\delta_{AMT}}} = \frac{dC_l}{d\delta_{AMT}}$$

and δ_{AMT} is the deflection of the AMTs.[8] Proper calculation of the stability derivative, from the linearization from which the stability derivative approach is derived, is to make $C_{l_{\delta_{AMT}}}$ a function of the control surface deflection angle and the remainder of the vehicle state, *i.e.*, α, β, Mach number, *etc.*. Unfortunately, it is not uncommon to simplify these relationships to the greatest extents possible if not forgo the process entirely, and make these coefficients constants with respect to some or all of the state variables. Such a simplification obviously reduces greatly the size of the database required for defining the vehicle's aerodynamic characteristics, and therefore the cost of developing this database.

From the review of the data presented in this report, the hazards in simplifying the aerodynamic model for control surface deflection effects are readily apparent. In these data a number of examples of nonlinear behavior are seen, indicating that at a minimum the control-surface-induced increment was a nonlinear function of the surface deflection magnitude. Furthermore, some instances of apparent discontinuities in the total response was seen to be added, deleted, or shifted with respect to angle of attack and/or sideslip. Obviously, the common practice of simplifying and minimizing the aerodynamic database for control surface deflection effects would cause these important effects to be overlooked, potentially adding significant costs from the need to redesign the flight control law – or possibly the vehicle itself – to correct for these omissions.

Without detailed flow visualization or flow survey data, determining the exact cause for the observed nonlinear and discontinuous behavior of these data is not possible; however, from previous experience a reasonable hypothesis may be generated. As is shown in Figure 27, the ICE 101 model's delta-wing planform generates a strong helical vortex along the leading edge (the leading-edge vortex, or LEV). Based on experience with a generic 65° delta wing,[3] flow field topology bifurcations, such as LEV burst and the formation and bursting of secondary vortex structures, may be anticipated to occur in the ICE 101-generated flow field. These phenomena and other such flow field bifurcations have been shown empirically to be associated with many critical states.[6] Given that deflections of the control surfaces modifies the local geometry of the body – and hence the local pressure profiles – the flow field topology can be anticipated to be functions of these deflections as it is a function of the angles of attack and sideslip (and the remainder of the state variables). This modification of the boundary conditions thus alters the dynamical system which defines the occurrence of topological bifurcations, and hence the occurrence of critical states.

Regardless of their exact cause, the manipulation of these nonlinear effects and apparent discontinuities has one important implication: the effects of critical states may be manipulated through the geometric alteration of the vehicle body. Although this result may be inferred from the copious studies of such phenomena as the effect of blowing on LEV burst point location, these results are direct evidence of the influence control surfaces have on aerodynamic nonlinearity. Further study of this causal relationship ought to lead to more elegant means of controlling these aerodynamic effects, either through tailoring of the control surface deflection schedule or possibly through micro-scale flow control and active wing shaping technology.

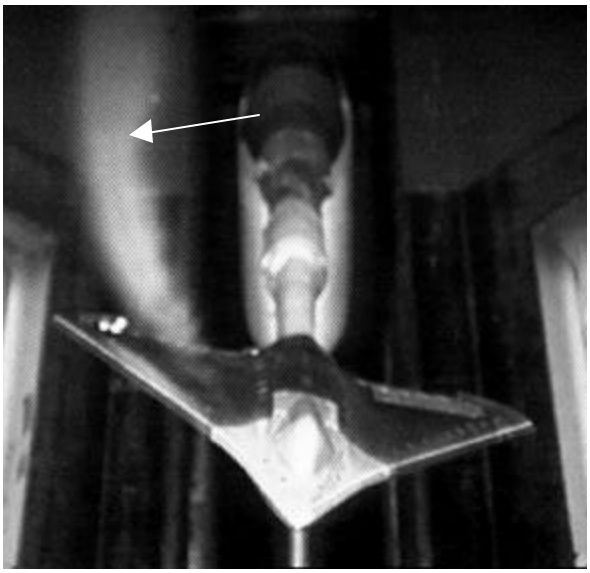

Figure 27 The ICE 101 Model in the SARL Wind Tunnel, Showing the LEV Structure
(Note the presence of LEV burst aft of the trailing edge (arrow).)

7.0 Summary

The data detailed in this report demonstrate the effect which control-surface deflection can have on the nonlinear aerodynamic forces and moments generated by the ICE 101's delta wing planform. Most significantly, a number of instances were found where possible discontinuities found in the baseline-configuration were moved in angle of attack or sideslip angle, or the effect was suppressed through deflection of a control surface. The majority of these instances were isolated to flight conditions centered on $\alpha = 25°$ and / or $\beta = 10°$, leading to the hypothesis that these results may be related to the presence of LEV burst over the planform. However, in the absence of flow field measurements and flow visualization, this hypothesis cannot be tested. In many other instances, few of which were discussed in the body of this report, the aerodynamic force and increments appeared to be nonlinear functions of angle of attack and sideslip angle.

These results are significant from the perspective of flight control since such aerodynamic characteristics are seldom provided for in flight control systems. They also suggest that such nonlinear effects may be manipulated using flow control devises at least on the macroscopic scale.

8.0 References

[1] Dorsett, K.M., and D.R. Mehl, "Innovative Control Effectors (ICE)," WL-TR-96-3043, Wright Laboratories, Wright-Patterson AFB, OH, January 1996.

[2] Dorsett, K.M., S.P. Fears and H.P. Houlden, "Innovative Control Effectors (ICE) Phase II," WL-TR-97-3059, Wright Laboratories, Wright-Patterson AFB, OH, July 1997.

[3] Jenkins, J.E., and E.S. Hanff, "Highlights of the IAR/WL Delta Wing Program," presented at Workshop III – Delta Wings: Unsteady Aerodynamics and Modeling, AIAA Atmospheric Flight Mechanics Conference, 8 August 1995.

[4] Jenkins, J.E., "Nonlinear Aerodynamic Characteristics of a 65 Degree Delta Wing in Rolling Motion: Implications to Testing and Flight Mechanics," AIAA Paper 97-0742, January 1997.

[5] Myatt, J.H., "A Nonlinear Indicial Response Model for the Rolling 65-Degree Delta Wing," AIAA Paper 96-3406, July 1997.

[6] Addington, G.A., The Role of Flow Structure in Determining the Aerodynamic Response of a Delta Wing, University of Notre Dame Ph.D. Dissertation, 1998.

[7] Gilliard, W., "Innovative Control Effectors (Configuration 101) Dynamic Wind Tunnel Test Report: Rotary Balance and Forced Oscillation Tests," AFRL-VA-WP-TR-1998-3043, July 1998.

[8] Nelson, Robert C., Flight Stability and Automatic Control, 2nd ed., McGraw-Hill, 1998.